Acoustic Radiation Force Impulse (ARFI) Prostate Zonal Anatomy: Comparison with Endorectal T2-Weighted MR Imaging (T2WI)

Mark L. Palmeri, M.D., Ph.D.*, Kirema Garcia-Reyes†, Stephen J. Rosenzweig*, Rajan Gupta, M.D.‡, Christopher Kauffman, M.D.‡, Thomas Polascik, M.D.§, Samantha L. Lipman*, Zachary A. Miller*, Tyler Glass*, Andrew Buck, M.D.¶, John Madden, M.D.¶, Kathryn R. Nightingale, Ph.D.*

*Department of Biomedical Engineering, Pratt School of Engineering, Duke University †Duke University School of Medicine ‡Department of Radiology, Duke University Medical Center §Department of Surgery (Urology), Duke University Medical Center ¶Department of Pathology, Duke University Medical Center

I. Keywords

Acoustic Radiation Force Impulse (ARFI) imaging, Magnetic Resonance (MR) imaging, T2-weighted imaging (T2WI), prostate, zonal anatomy

II. Introduction

The introduction text will go here. AHHHHHH

III. Background

A. Prostate Anatomy

The prostate gland sits below the urinary bladder and surrounds the urethra. Its superior borders include the bladder and seminal vesicles and the urogenital diaphragm delineates its inferior boundary. The gland is bordered anteriorly by the pubic symphysis and posteriorly by the rectum. The prostate is separated from the rectum by 2–3 mm fascial layer, [1] and can be easily palpated on rectal examination.

The gland can be divided from superior to inferior into the base, midgland and apex. The urethra enters the prostate proximally at the base and extends to the midgland at which point the ejaculatory ducts open into the urethra at the verumontanum. [1] The urethra then continues past the apex and travels through the penis. The prostate can be divided into glandular and non-glandular components. The glandular components include the transitional zone,

central zone and peripheral zone. Each zone contains approximately 5%, 20% and 70–80% of glandular tissue, respectively. [2] The non-glandular components include the anterior fibromuscular stroma and the urethra.

Although not a true capsule, an outer band of fibromuscular tissue surrounds the prostate. [2] This "capsule" is important when assessing the extraprostatic extension of cancer as tumor can spread by disrupting this tissue. Two neurovascular bundles course posterior and lateral to the prostate, which can also be invaded by malignant cells.

B. Clinical Background and Significance

Prostate cancer (PCa) is the most common noncutaneous malignancy among men in the United States. Approximately 1 in every 6 men will develop PCa during their lifetime, with the median age of diagnosis at 67. 1It is also the second leading cause of cancer related death, with 1 in 36 men dying from the disease. The National Cancer Institute estimates that 238,590 men will be diagnosed with PCa in 2013 and 29,720 will die from the disease. [3]

PCa diagnosis usually begins by screening with prostate specific antigen (PSA) and digital rectal examination (DRE). Definitive diagnosis is made by random transrectal ultrasonography-guided (TRUS) biopsies, which are then used to provide the clinician with the proper Gleason score. The combination of these factorsas well as stagingdetermines the appropriate therapy and prognosis.

PCa screening has led to earlier diagnosis of smaller tumors and more localized disease. However, it is well known that the sensitivity and specificity of PSA and DRE are not optimal. In addition, DRE has a low predictive value at lower PSA ranges, and PSA yields many false positives. [4], [5], [6] As such, a theoretical risk of over-diagnosis and treatment of low-gradeand possibly clinically insignificantdisease exists. Moreover, due to the random nature of biopsies, cancer located outside the routine sampling site can be missed and the extent of the cancer might be underestimated. [5], [**?**] For example, in a study by Mufarrij et al 45.9–47.2% of patients who were candidates for active surveillance but underwent radical prostatectomy had a higher Gleason score on final histopathology than after TRUS biopsy. [7] These inaccuracies may lead to inappropriate diagnosis, imprecise risk assessment and potentially avoidable morbidity.

The Use of Magnetic Resonance Imaging in Prostate Diagnostics

Magnetic resonance (MR) imaging has been available for use in the workup of patients with PCa since the early 1980s but the early work on its diagnostic accuracy is heterogeneous.7 Earlier MR techniques relied mostly on morphology via T1 and T2- weighted imaging (T2WI). The more recent ability to include not only anatomic but also biologic and functional dynamic parameters into MR analysisvia diffusion-weighted imaging (DWI), dynamic contrast-enhanced (DCE) imaging or MR spectroscopic imaging (MRSI)is promising in the future diagnosis and management of PCA.

Currently prostate MR focuses on a multiparametric approach, where 2 or more imaging sequencesincluding anatomic and functional dataare used together to try to arrive to a diagnosis. [8] As MR technology continues to evolve and improve, its role in PCA diagnosis, staging, treatment planning and follow-up has gained much attention.

C. T2-Weighted Imaging and Prostate Anatomy

T2WI sequences are crucial components of prostate MR imaging. T2WI is particularly useful in prostate analysis due to its excellent soft tissue contrast resolution, which can be maximized by using thin sections of 3–4 mm and a small field of view of approximately 14 cm. [5], [2] T2 sequences are the most helpful for tumor localization as they can clearly show overall prostate morphology, internal structures and prostatic margins. [5]

The prostate can be divided into glandular and nonglandular components. The glandular components include the peripheral zone (PZ) and the central gland, which are typically easily distinguishable on T2WI. The central gland includes the central zone, transition zone and the periurethral glandular tissue. [1] Other anatomical markers such as the urethra, verumontanum and ejaculatory are also often seen on T2WI.

Approximately 70% of the prostatic tissue is found in the peripheral zone, which is high in water content and thus of higher signal intensity in T2WI. [1] Seventy five percent of prostatic tumors are found in the PZ and normally show hypointense T2 signal when compared to the higher intensity PZ. [6], [9] However, tumors can sometimes seem of similar intensity as the surrounding tissue and false positives can occur secondary to post biopsy changes/hemorrhage, hyperplasia or prostatitis, making diagnosis more challenging. [9]

D. Functional MR Sequences

Even though T2WI is the mainstay of prostate MR, its overall performance in prostate cancer diagnosis is not optimal. The incorporation of two or more functional sequences in multiparametric MR imaging (mpMRI) has been shown to significantly improve the performance of MRI in cancer diagnosis. [10] In fact, the European Society of Urogenital Radiologys (ESUR) prostate MR guidelines recommend at least 2 functional imaging techniques in addition to T2WI in order to better characterize prostate tumors. [8] In a study by Turkbey et al., researchers found that mpMRI had a positive predictive value of 98% in prostate cancer detection. [10] Functional sequences include diffusion- weighted imaging (DWI), dynamic contrast enhanced imaging (DCE-MRI) and MR spectroscopic imaging (MRSI).

E. Diffusion-weighted imaging

DWI is based on the free movement of water particles in tissue and measures the degree of motion restriction. [11] Normal prostatic tissue is very glandular with plenty of water molecule movement. On the other hand, tumors have high cellular density and restricted water movement, which leads to decreased diffusion. Due to this restricted diffusion, tumors seem to be of higher intensity on DWI. [11]

DWI sequences can be processed to obtain apparent diffusion coefficient (ADC) maps. These serve as a more objective measure of diffusivity since they are independent of magnetic field and thus overcome the effects of T2 shine-through. [10], [11] ADC maps are also used to visually assess the tumor, which appears as a focus of decreased signal intensity when compared to normal prostate tissue. [12]

In addition to knowing the location of the cancer within the prostate, being able to identify which cancers will exhibit more aggressive behavior is important when making clinical management decisions. A number of studies

have found that lower ADC values correlate with tumors that have higher Gleason scores. [13], [**?**], [14] This could be explained by the fact that higher-grade lesions are usually of higher cellular density and thus have even more marked restricted diffusion. This inverse correlation suggests that ADC maps might be helpful when characterizing lesions and assessing tumor aggressiveness. [15]

F. Dynamic contrast enhanced imaging

DCE-MRI has been shown to have a high sensitivity in cancer detection, especially when combined with other MR imaging modalities. [16], [17], [18], [19] In a study by Hara et al, this functional modality identified 93% of clinically significant cancers. [20] DCE-MRI provides a measure of tumor vascularity and takes advantage of tumor-induced angiogenesis in PCa. [21] Increased vascularity in PCa results in earlier and higher peak contrast enhancement and a faster washout when compared to normal prostatic tissue. These known characteristics of PCa are helpful when trying to localize lesions.

A variety of different approaches can be used to analyze DCE-MRI and no report has, up to date, described the superiority of one method over the others. [5] The approaches include qualitative analysis by visual assessment of the images, semi-quantitative methods that look at kinetic parameters on a voxel-by-voxel basis, or quantitative methods that that convert signal intensity into kinetic parameters to determine how much contrast is being exchanged between the vascular, extravascular and extracellular spaces. [5]

G. MR spectroscopy

Like DWI, MRSI can be helpful in lesion characterization as it provides information on the presence of certain metabolites in tissue. [8] Choline and citrate are especially useful in the setting of PCa. Choline is critical in cell membrane synthesis and is thus usually elevated in cells with cancerous behavior.3 Healthy prostate epithelium synthesizes and secretes large quantities of citrate but levels are decreased in PCa. [22], [23] Therefore, an increase in the choline-to-citrate ratio on MRSI can be used as an indicator of malignancy. [2]

Although some data suggests that MRSI increases the accuracy of tumor volume detection and staging when used in addition to anatomic imaging, it is unclear whether it is superior to other modalities. [2] ESUR lists MSRI as an optional modality for the diagnosis of PCa since it significantly lengthens exam time and requires specific technical expertise. [8] Thus, it is not surprising that many academic centers in the United States do not include MSRI in their mpMRI prostate cancer protocols. [5]

IV. METHODS

A. Study Inclusion Criteria & MR Imaging

Prostates removed by radical prostatectomy were used in this IRB-approved (Duke IRB# Pro00006458), HIPAA-compliant study from men ranging in age from XX–XX diagnosed with biopsy-proven prostate cancer destined for surgical removal. Between DATES, a total of XX patients were recruited and enrolled in this study. Inclusion criteria were undergoing complete pelvic MRI with endorectal coil for detection of prostate cancer, including multiplanar

T2-weighted anatomic imaging, diffusion-weighted imaging (DWI), and dynamic contrast enhanced MRI (DCE-MRI) as well as radical prostatectomy and whole mount histology. Patients with previous treatments of prostate cancer or benign prostatic hyperplasia (BPH), or anatomic anomalies of the rectum, were excluded. All patients enrolled in this study provided written informed consent. Our final cohort included XX subjects. Table XX has a summary of the patient demographics for the cases shown in this manuscript.

All imaging was performed on one of two 3.0 Tesla MR scanners (General Electric HDx, GE Healthcare, Waukesha, WI; Siemens Skyra, Siemens Healthcare, Erlangan, Germany) using a single channel Medrad eCoil endorectal coil (Medrad, Indianola, PA) as well as multichannel surface coils. Imaging sequences included thin-section (3 mm section thickness) fast spin echo T2-weighted images in the coronal, axial and sagittal planes. Diffusion weighted images were obtained using multiple b-values and calculation of ADC maps was also performed. Dynamic contrast enhanced MR sequences were obtained after administration of a weight-based dose of extracellular MR contrast agent with 4-5 second temporal resolution for 5-6 minutes. (If we need it, can put in table with full MR parameters) Prostates were radically removed using a da Vinci Surgical System (INSERT COMPANY INFORMATION). After exision, the prostates were formalin fixed for at least 24 hours without being cut, and then processed for whole mount histology.

B. ARFI Imaging Methods

Experimental ARFI imaging data were acquired using a modified Siemens Acuson SC2000 ultrasound scanner (Siemens Healthcare, Ultrasound Business Unit, Mountain View, CA, USA) and the longitudinal array of an Acuson ER7B transducer [**?**]. The ARFI imaging sequence was comprised of standard B-mode ultrasonic imaging, or tracking beams, and pushing beams. For each lateral location, two pre-push reference images were acquired, then three 300 cycle pushing pulses were transmitted in rapid succession, focused at 30 mm, 22.5 mm, and 15 mm, respectively, and finally the response of the tissue was tracked for up to 6ms at a PRF of 8kHz. This pushing strategy is similar to what has been published by Bercoff et al [**?**]. The 30 mm and 22.5 mm foci pushing pulses were transmitted at 4.6 MHz with a F/2 geometry and the 15 mm focus pushing pulse was transmitted at 5.4 MHz with a F/2.35 geometry to maintain the same beamwidth (0.67 mm) throughout the region of excitation. A total of 82 lateral locations were interrogated to cover the 55 mm field of view, translating 0.67 mm laterally per location.

For the tracking pulses, 16 parallel receive lines at 5.0 MHz were spaced to observe both the on and off-axis response of the tissue to the pushing pulses. Specifically, four lines were dedicated to tracking the on-axis displacement, with all 4 beams located inside the beamwidth of the pushing pulses such that the beam spacing was 0.17 mm. The other twelve lines were separated into two groups to observe both the left and right propagating waves. For each sub-group of 6, the beams were located 1.89 mm laterally offset from the push and had an inter-beam spacing of 0.76 mm to cover a total field of view of 11.3 mm laterally. For brevity, the 4 on-axis beams will be referred to as the ARFI data and the 12 off-axis beams will be referred to as the SWEI data.

Displacement estimation was performed using a phase shift estimator on the beamformed IQ data [**?**], [**?**]. The ARFI data were then normalized as a function of depth to account for attenuation and focal gain effects by taking

the mean displacement across the entire data set at each time step then low-pass filtering with a cutoff frequency of 0.8 mm^{-1}.

C. Image Zonal Anatomy Segmentation and 3D Model Rendering

Axial T2W MR slices were manually segmented using the polygon tool on ITK SNAP using separate labels for the peripheral zone (PZ), central gland (CG) and anterior fibromuscular stroma (AFS). The gland was segmented from base to apex. The base was identified below the bladder and subsequent images were segmented until the last slice with visible prostatic tissue was identified caudally. The CG, PZ and AFS were segmented independently according to their well-established anatomical characteristics on T2WI. [**?**], [1], [24], [6], [2] The PZ was identified by its homogenous high signal intensity on T2WI, which is usually similar to that of the nearby periprostatic fat. The CG was visualized and delineated based on its heterogeneous and lower signal intensity as well as its location. Although not readily visible on every case, the AFS was identified by its low T2 signal intensity and its location anterior to the central gland.

V. Results

- Images of select cases, demonstrating segmentation process

The computed volumes of the prostates from the MR and ARFI imaging data are presented in Table **??**. The subvolumes associated with the zonal anatomy in each imaging modality was measured (Figure **??**(a)), showing an mean overestimation of total prostate volume of 36.7 $\pm$ 27.9% by ARFI imaging compared to MR volumes (Figure **??**(b)), and a relative underestimation of the central zone volume relative to the central gland in MR imaging of -15.3 $\pm$ 13.0 % (Figure **??**(c)).

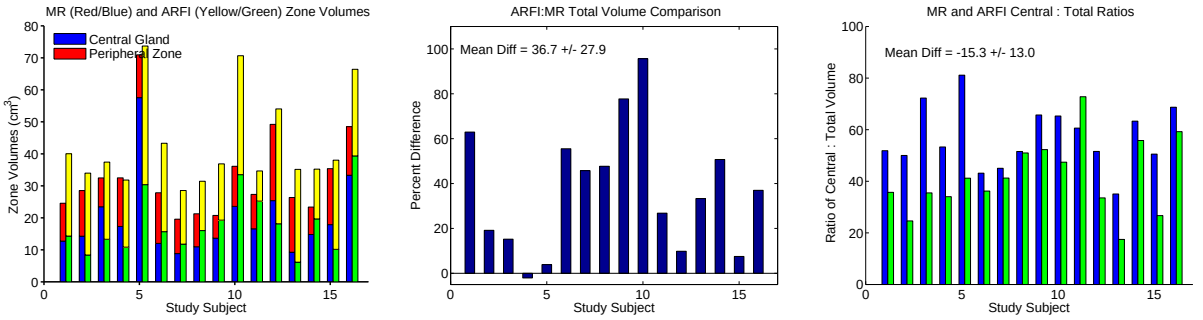

(a) Central:Peripheral Volume (b) Total Volume Difference (c) Central:Total Volume Difference

Fig. 1. Comparison of MR and ARFI zonal anatomy volume estimates from manually-segmented images. Total prostate volumes ranged from 19.6–71.0 cm^3 based on MR image models (a), with ARFI image models overestimating total prostate volume by 36.7 $\pm$ 27.9% (b). ARFI image delineation of the central zone volume relative to total prostate volume showed a mean underestimation of -15.3 $\pm$ 13.0% (c, green) relative to the MR central gland : total volume ratios (c, blue).

Weights and axis measurements from the gross pathology processing of the excised prostates were collected (Table II), and using the axis measurements (lateral-to-lateral, anterior-to-posterior, and apex-to-base), the prostate volume was approximated as a tri-axial ellipsoid, and its volume was estimated.

TABLE I
COMPARISON OF CENTRAL GLAND / ZONE AND TOTAL PROSTATE VOLUMES IN MR T2WI AND ARFI IMAGING

Study Subject	**MR Central Gland Volume (cm^3)**	**MR Total Volume (cm^3)**	**ARFI Central Zone Volume (cm^3)**	**ARFI Total Volume (cm^3)**
1	12.74	24.57	14.30	40.03
2	14.26	28.51	8.37	33.98
3	23.47	32.48	13.29	37.42
4	17.32	32.49	10.83	31.82
5	57.56	70.95	30.37	73.68
6	12.01	27.84	15.68	43.30
7	8.82	19.59	11.78	28.55
8	10.97	21.28	16.02	31.42
9	13.63	20.75	19.28	36.88
10	23.58	36.11	33.50	70.65
11	16.57	27.33	25.22	34.66
12	25.38	49.21	18.14	54.04
13	9.25	26.36	6.14	35.14
14	14.79	23.36	19.65	35.21
15	17.87	35.37	10.15	38.03
16	33.32	48.50	39.35	66.42

TABLE II
PATHOLOGY PROSTATE GROSS SPECIMEN METRICS

Study Subject	**Weight (g)**	**Lat-Lat (cm)**	**Anterior-Posterior (cm)**	**Apex-Base (cm)**	**Ellipsoidal Volume (cm^3)**
1	37.	4.3	4.0	2.9	26.10
2	52.	4.5	3.5	3.5	28.85
3	38.	4.5	4.0	3.7	34.85
4	84.	7.0	6.5	6.0	142.87
5	72.	6.6	4.3	3.0	44.56
6	49.	4.9	4.4	3.4	38.36
7	25.	3.7	3.7	3.2	22.93
8	27.	4.2	3.1	2.7	18.40
9	28.	4.4	3.7	3.2	27.26
10	42.	4.7	3.5	3.2	27.55
11	38.	5.4	4.0	3.3	37.30
12	50.	5.0	4.0	3.7	38.73
13	29.	4.0	3.5	3.0	21.98
14	27.	4.5	3.0	3.0	21.20
15	32.	4.5	3.5	3.5	28.85
16	62.	5.5	5.3	5.2	79.33

MR and ARFI imaging total prostate volumes were also compared with the weights and prostate volumes, approximated to be tri-axial ellipsoids, and calculated from measurements of the prostate semi-principal axes. Prostate weights were moderately correlated with estimated pathology ellipsoidal prostate volumes (Figure 2(a), R^2 = 0.68). There was moderate correlation between the prostate weight and the image-reconstructed prostate volumes (Figure 2(b), R^2 = 0.44 (MR) and 0.21 (ARFI)), though there was weaker correlation with the ellipsoidal approximation of the measurement prostate volume and the image-recontructed volumens (Figure 2(c), R^2 = 0.08 (MR) and 0.01 (ARFI)).

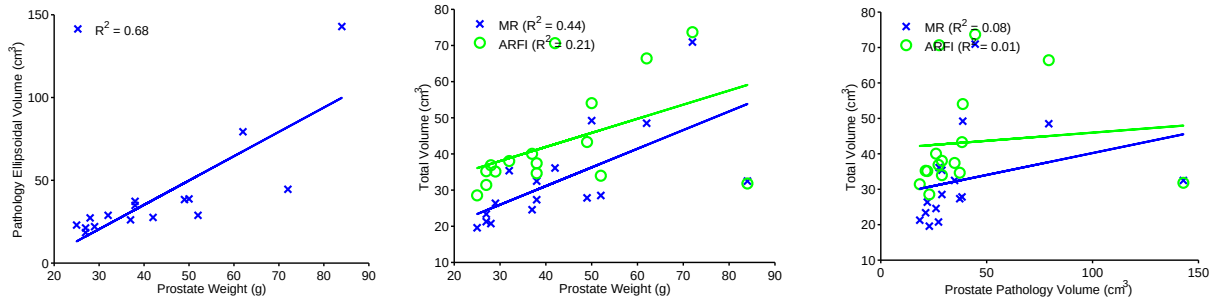

(a) Path Weight : Path Volume (b) Image Volume : Prostate Weight (c) Image Volume : Path Volume

Fig. 2. Tri-axial pathology measurements were used to make an ellipsoidal prostate volume approximation based on gross pathology axis measurements, which was moderately well-correlated with the excised prostated weights (a, R^2 = 0.68). T2WI MR (blue, X) showed a moderate correlation between the reconstructed volumes and prostate weight (R^2 = 0.44), while volumes reconstructed from ARFI images (green, O) showed weaker correlation (R^2 = 0.21) (b). Even weaker correlations existed between both T2WI MR and ARFI image volumens and approaximated ellipsoidal prostate pathology volumes (R^2 = 0.08 and 0.01, respectively) (c).

VI. Discussion

- BPH and PCa can heavily compromise ability to see zones. No healthy prostates were studied, which would have made this analysis easier; however, the prostate of the older man, which would be in our screening population, is not that of the healthier, younger male, making analysis in that population less meaningful.

VII. Conclusions

The delineation of prostate zonal anatomy in ARFI images has been compared with the established methods for identifying zonal anatomy using T2 MR images. In XX cases of prostates containing varying degrees of PCa and BPH, perpipheral zone volumes…XXXXX and central gland volumes…XXXXX. Aspect ratios of the central glad agreed to within XX% between MR and ARFI imaging datasets. Appreciable amounts of BPH made determining the transition between the central gland and peripheral zone difficult to discern and, these cases were not included in this analysis. Additionally, large PCa lesions can also distort prostate zonal anatomy appreciably, making the distinction between peripheral zone and central gland challenging. Overall, ARFI imaging is able to delineate central gland from peripheral zone in the prostate in the absence of excessive BPH or PCa tumor burden.

TABLE III
COMPARISON OF CENTRAL GLAND / ZONE (C) AND TOTAL (T) PROSTATE AXES IN MR T2WI AND ARFI IMAGING. AXES ARE APPROXIMATED IN ORIENTATION TO MATCH THOSE SPECIFIED IN GROSS PATHOLOGY: LATERAL-TO-LATERAL (LL), ANTERIOR-TO-POSTERIOR (AP) AND APEX-TO-BASE (AB).

Study Subject	**MR C-AB (cm)**	**ARFI C-AB (cm)**	**MR C-LL (cm)**	**ARFI C-LL (cm)**	**MR C-AP (cm)**	**ARFI C-AP (cm)**	**MR T-AB (cm)**	**ARFI T-AB (cm)**	**MR T-LL (cm)**	**ARFI T-LL (cm)**	**MR T-AP (cm)**	**ARFI T-AP (cm)**
1	4.12	4.34	2.90	3.51	2.45	2.28	4.12	5.26	3.80	4.94	3.09	3.14
2	3.87	4.03	3.39	3.25	2.80	1.66	3.87	3.06	4.45	5.46	3.59	3.86
3	4.82	4.53	3.48	3.23	3.27	2.29	5.11	4.53	4.11	4.55	3.59	3.68
4	5.35	3.82	3.08	2.62	2.87	2.35	5.36	4.18	4.45	4.63	3.37	3.66
5	6.22	5.20	4.66	5.06	4.98	2.42	7.39	5.20	5.43	6.24	5.63	4.28
6	5.05	4.63	3.44	3.96	3.44	2.29	5.10	4.50	4.84	5.83	3.44	3.10
7	4.47	4.77	3.33	3.42	2.26	2.40	4.72	3.92	4.44	4.80	2.58	2.84
8	4.30	5.72	3.20	4.23	2.10	2.52	4.32	4.50	4.23	4.71	2.48	2.97
9	3.52	4.73	3.31	4.90	2.19	2.69	3.52	4.43	4.33	5.71	2.70	3.06
10	5.24	5.02	4.43	7.19	2.69	2.20	5.23	4.85	5.15	7.46	3.37	3.20
11	5.02	4.24	3.85	4.31	2.73	2.72	5.02	3.15	5.50	5.16	3.57	2.78
12	4.55	4.24	3.70	4.63	3.30	2.34	4.58	3.87	5.38	6.74	4.24	3.83
13	3.40	2.84	4.03	3.29	2.01	1.91	4.08	3.89	4.72	5.31	2.94	3.46
14	3.56	4.18	3.69	4.84	2.54	2.29	3.56	4.14	4.33	5.04	3.17	3.02
15	4.79	5.00	4.17	3.78	2.56	3.08	4.95	4.12	4.69	5.31	3.32	3.60
16	5.11	5.03	4.60	6.14	3.11	3.13	5.12	4.61	5.62	6.23	3.71	3.52

ACKNOWLEDGEMENTS

The authors would like to thank Siemens Medical Solution USA, Ultrasound Division for their in-kind technical support and Ned Danieley for computer system administration support. This work was supported by NIH R01CA142824 and the Duke Coulter Translational Grant Program.

DISCLOSURES

Some of the authors on this manuscript hold intellectual property related to ARFI imaging, and commercial licenses of this technology with Duke University exist. There are no personal financial disclosures for the authors.

REFERENCES

[1] A. J. Jung and A. C. Westphalen, "Imaging Prostate Cancer," *Radiologic Clinics of North America*, vol. 50, no. 6, pp. 1043–8389, 2012.

[2] D. Bonekamp, M. A. Jacobs, R. El-Khouli, D. Stoianovici, and K. J. Macura, "Advancements in MR imaging of the prostate: from diagnosis to interventions," *Radiographics*, vol. 31, no. 3, pp. 677–5333, 2011.

[3] N. Howlader, A. M. Noone, M. Krapcho, N. Neyman, R. Aminou, and W. Waldron, "SEER Cancer Statistics Review, 19752010, National Cancer Institute. Bethesda, MD, based on November 2012 SEER data submission, posted to the SEER web site, 2013," *http://seer.cancer.gov/csr/1975_2010 (Accessed on June 08, 2013)*, 2011.

[4] C. Gosselaar, M. J. Roobol, S. Roemeling, T. H. van der Kwast, and F. H. Schröder, "Screening for prostate cancer at low PSA range: the impact of digital rectal examination on tumor incidence and tumor characteristics," *The Prostate*, vol. 67, no. 2, pp. 45–154, 2007.

[5] R. T. Gupta, C. R. Kauffman, T. J. Polascik, S. S. Taneja, and A. B. Rosenkrantz, "The state of prostate MRI in 2013," *Oncology (Williston Park)*, vol. 27, no. 4, pp. 262–270, 2013. [Online]. Available: http://www.ncbi.nlm.nih.gov/pubmed/23781689

[6] H. Hricak, P. L. Choyke, S. C. Eberhardt, S. A. Leibel, and P. T. Scardino, "Imaging prostate cancer: A multidisciplinary perspective1," *Radiology*, vol. 243, no. 1, pp. 28–8419, 2007.

[7] P. Mufarrij, A. Sankin, G. Godoy, and H. Lepor, "Pathologic outcomes of candidates for active surveillance undergoing radical prostatectomy," *Urology*, vol. 76, no. 3, pp. 689–4295, 2010.

[8] J. O. Barentsz, J. Richenberg, R. Clements, P. Choyke, S. Verma, G. Villeirs, O. Rouviere, V. Logager, and J. J. Fütterer, "ESUR prostate MR guidelines 2012," *European radiology*, vol. 22, no. 4, pp. 746–7994, 2012.

[9] J. V. Hegde, R. V. Mulkern, L. P. Panych, F. M. Fennessy, A. Fedorov, S. E. Maier, and C. Tempany, "Multiparametric MRI of prostate cancer: An update on stateoftheart techniques and their performance in detecting and localizing prostate cancer," *Journal of Magnetic Resonance Imaging*, vol. 37, no. 5, pp. 1035–2586, 2013.

[10] B. Turkbey and P. L. Choyke, "Multiparametric MRI and prostate cancer diagnosis and risk stratification," *Current opinion in urology*, vol. 22, no. 4, pp. 310–643, 2012.

[11] D.-M. Koh and D. J. Collins, "Diffusion-weighted MRI in the body: applications and challenges in oncology," *American Journal of Roentgenology*, vol. 188, no. 6, pp. 1622–1635 %@ 0361–803X, 2007.

[12] C. H. Tan, J. Wang, and V. Kundra, "Diffusion weighted imaging in prostate cancer," *European radiology*, vol. 21, no. 3, pp. 593–7994, 2011.

[13] T. Kobus, P. C. Vos, T. Hambrock, M. De Rooij, C. A. HulsbergenVan de Kaa, J. O. Barentsz, A. Heerschap, and T. W. J. Scheenen, "Prostate cancer aggressiveness: in vivo assessment of MR spectroscopy and diffusion-weighted imaging at 3 T," *Radiology*, vol. 265, no. 2, pp. 457–8419, 2012.

[14] T. Hambrock, D. M. Somford, H. J. Huisman, I. M. van Oort, J. A. Witjes, C. A. Hulsbergen-van de Kaa, T. Scheenen, and J. O. Barentsz, "Relationship between apparent diffusion coefficients at 3.0-T MR imaging and Gleason grade in peripheral zone prostate cancer," *Radiology*, vol. 259, no. 2, pp. 453–8419, 2011.

[15] H. A. Vargas, O. Akin, T. Franiel, Y. Mazaheri, J. Zheng, C. Moskowitz, K. Udo, J. Eastham, and H. Hricak, "Diffusion-weighted endorectal MR imaging at 3 T for prostate cancer: tumor detection and assessment of aggressiveness." *Radiology*, vol. 259, no. 3, pp. 775–84, Jun. 2011. [Online]. Available: http://radiology.rsna.org/content/259/3/775.full

[16] A. Tanimoto, J. Nakashima, H. Kohno, H. Shinmoto, and S. Kuribayashi, "Prostate cancer screening: The clinical value of diffusionweighted imaging and dynamic MR imaging in combination with T2weighted imaging," *Journal of Magnetic Resonance Imaging*, vol. 25, no. 1, pp. 146–2586, 2007.

[17] N. Girouin, F. Mège-Lechevallier, A. T. Senes, A. Bissery, M. Rabilloud, J.-M. Maréchal, M. Colombel, D. Lyonnet, and O. Rouvière, "Prostate dynamic contrast-enhanced MRI with simple visual diagnostic criteria: is it reasonable?" *European radiology*, vol. 17, no. 6, pp. 1498–7994, 2007.

[18] I. Ocak, M. Bernardo, G. Metzger, T. Barrett, P. Pinto, P. S. Albert, and P. L. Choyke, "Dynamic contrast-enhanced MRI of prostate cancer at 3 T: a study of pharmacokinetic parameters," *American Journal of Roentgenology*, vol. 189, no. 4, pp. W192–W201 %@ 0361–803X, 2007.

[19] J. K. Kim, S. S. Hong, Y. J. Choi, S. H. Park, H. Ahn, C. Kim, and K. Cho, "Washin rate on the basis of dynamic contrastenhanced MRI: Usefulness for prostate cancer detection and localization," *Journal of Magnetic Resonance Imaging*, vol. 22, no. 5, pp. 639–2586, 2005.

[20] N. Hara, M. Okuizumi, H. Koike, M. Kawaguchi, and V. Bilim, "Dynamic contrastenhanced magnetic resonance imaging (DCEMRI) is a useful modality for the precise detection and staging of early prostate cancer," *The Prostate*, vol. 62, no. 2, pp. 45–140, 2005.

[21] S. M. Noworolski, R. G. Henry, D. B. Vigneron, and J. Kurhanewicz, "Dynamic contrastenhanced MRI in normal and abnormal prostate tissues as defined by biopsy, MRI, and 3D MRSI," *Magnetic resonance in medicine*, vol. 53, no. 2, pp. 249–2594, 2005.

[22] L. C. Costello, , R. B. Franklin, and P. Narayan, "Citrate in the diagnosis of prostate cancer," *The Prostate*, vol. 38, no. 3, pp. 45–237, 1999.

[23] J. Kurhanewicz, M. G. Swanson, S. J. Nelson, and D. B. Vigneron, "Combined magnetic resonance imaging and spectroscopic imaging approach to molecular imaging of prostate cancer," *Journal of Magnetic Resonance Imaging*, vol. 16, no. 4, pp. 451–2586, 2002.

[24] P. Y. Poon, R. W. McCallum, M. M. Henkelman, M. J. Bronskill, S. B. Sutcliffe, M. A. Jewett, W. D. Rider, and A. W. Bruce, "Magnetic resonance imaging of the prostate," *Radiology*, vol. 154, no. 1, pp. 143–8419, 1985.